Bioactive Materials 41 (2024) 30–45

Contents lists available at ScienceDirect

Bioactive Materials

journal homepage: www.keaipublishing.com/en/journals/bioactive-materials

Thermo-sensitive Poloxamer based antibacterial anti-inflammatory and photothermal conductive multifunctional hydrogel as injectable, in situ curable and adjustable intraocular lens

Chen Qin, Fan Fei, Youfei Wei, Yuemei Han, Di Hu, Quankui Lin *

National Engineering Research Center of Ophthalmology and Optometry, School of Biomedical Engineering, School of Ophthalmology and Optometry, Eye Hospital, Wenzhou Medical University, Wenzhou, 325027, China

ARTICLE INFO

Keywords:
Adjustable IOL
Injectable hydrogel
Antibacterial
Anti-inflammatory

ABSTRACT

Cataract patients look forwards to fewer postoperative complications and higher vision quality after surgery. However, the current intraocular lens (IOL) implanted after cataract surgery neither can adjust focal length in response to ciliary muscle contraction as natural lens nor have the ability to prevent postoperative complications. Herein, a thermosensitve Poloxamer based hybrid hydrogel with antibacterial anti-inflammatory and photothermal functional elements doping was designed and used as injectable, in situ curable, and adjustable IOL (FHTAB IOL). The FHTAB IOL was composed of thermosensitve triblock-polymer F127DA and a small amount of HAMA, combined with BP NS, TA, and Ag NPs. FHTAB IOL can be injected into the empty lens capsule after cataract surgery via an injectable thermos-gel under NIR illumination and then be rapidly cured to form a full-size IOL under short-time blue light irradiation. The designed injectable FHTAB IOL possesses high transparency and transmittance, with a refractive index similar to the natural lens and adjustable properties. It was stabilized as a refractive medium without any leakage in the eye. In addition, the TA and Ag NPs loaded in the FHTAB IOL displayed significant antibacterial and anti-inflammatory effects in vitro and vivo. This study presents a potentially effective new strategy for the development of multifunctional adjustable IOLs.

1. Introduction

Nowadays, cataract remains the leading cause of reversible visual impairment worldwide [1–3]. Phacoemulsification for opaque lens removal followed with intraocular lens (IOL) implantation is still the most common and effective cataract treatment strategy [4]. The IOL is used to replace the natural lens' refractive function in the eye [5]. Patients recover their vision well after IOL implantation, yet they may also face postoperative problems such as posterior capsule opacification (PCO), infection and inflammation [6,7]. Many researchers, including ourselves, were focused on the improvement the IOLs materials with lower complication occurrence [8–12]. Besides, the improvement of ocular accommodation has also gained attentions due to the increasing demand for high-quality vision [13].

To provide better vision, two new types of IOLs have been developed, namely extended depth of focus IOL (EDOF IOL) and adjustable IOL (or called as accommodative IOL, A-IOL). Different from mono- or tri-focal IOL which can only provide fixed focus at one or three distances, EDOF IOL extends the depth of focus using specially designed wavefront surfaces, which provide the ability to focus continuously from distance to near [14]. However, apart from the expensive IOL price, implantation of EDOF IOL also requires extremely high surgery skill requirements to avoid eccentricity. A-IOLs adjust vision by specially designed IOL that can be immobilized in different positions [15]. While its adjustment distance is still limited. Similar to the natural lens, the ideal A-IOL would provide dynamic refractive power by contracting and relaxing the ciliary muscles [16]. The injectable IOL provides a full-size lens replacement by injecting the fluid IOL material through a 1.2 mm incision into the lens capsule and then forming a solid body [17]. This kind of IOL is usually softer and responds to the ciliary muscle movement, and which overcomes the eccentricity of conventional IOL implantation. However, liquid IOL materials are prone to leakage before curing, which impedes its application.

The IOL materials are a limiting factor in the development of ideal A-

Peer review under responsibility of KeAi Communications Co., Ltd.
* Corresponding author.
E-mail address: linqk@wmu.edu.cn (Q. Lin).

https://doi.org/10.1016/j.bioactmat.2024.07.005
Received 11 March 2024; Received in revised form 1 July 2024; Accepted 4 July 2024
2452-199X/© 2024 The Authors. Publishing services by Elsevier B.V. on behalf of KeAi Communications Co. Ltd. This is an open access article under the CC BY-NC-ND license (http://creativecommons.org/licenses/by-nc-nd/4.0/).

IOL. The first generation of IOL was made of polymethylmethacrylate [18]. Subsequently, hydrophilic or hydrophobic acrylate polymer with a higher refractive index was developed as the second generation IOL materials, which was foldable and alleviated large cornea incision during the surgery [19–21]. But, despite all these, the current IOLs are still too stiff to deform with ciliary muscle movements, resulting in fixed focal length and lack the ability to adjust focus for different distances [22,23]. Thus, appropriate IOL materials that can dynamically adjust to ciliary muscle movements are on great demand.

On the other hand, postoperative intraocular inflammation and infection are another factor that should not be ignored. Symptoms may include photophobia, decreased vision, increased secretion, and swelling of the eye. Furthermore, Arnaud et al. demonstrated that several inflammation cytokines including IL-1β, IFN-γ, TNF-α, and IL-6 were found to increase in aqueous humor and were associated with the PCO development [24]. Infectious inflammation is most severe in the case of endophthalmitis, which is typically caused by bacterial infection and can result in blindness in severe cases. Postoperative intraocular inflammation and infection are typically treated with anti-inflammatory or antibiotic eye drops. However, the physiological barriers on the ocular surface make it difficult to be absorbed, which leads to low utilization and requires frequent administration. This challenged patient compliance. Therefore, the injectable IOL materials combined with anti-inflammatory and antibacterial properties may be a charming way to combat postoperative complications.

F127DA is the polyethylene oxide (PEO)-polypropylene oxide (PPO)-PEO triblock polymer (also called Poloxamer) with acrylate group endings that can self-assemble with temperature changing to form hydrogels with excellent mechanical and injection properties [25]. Upon light curing, it exhibits low swelling, fatigue resistance, and an appropriate elastic modulus. Tannic acid (TA) is a natural polyphenol and a derivative of gallic acid. It contains several gallic acid groups in its structure. TA can interact with various organic, inorganic, hydrophilic, and hydrophobic substances through hydrogen, electrostatic, and ligand bondings as well as hydrophobic interactions. It has been widely used in biomedical applications as a natural cross-linking agent with anti-inflammatory, antibacterial, and anticancer activities [26,27]. Black phosphorus nanosheet (BP NS) is a kind of two-dimensional materials. The high surface area and energy conversion efficiency of BP NS enable them significant photothermal effects [28]. In the presence of light and an oxygenated environment, the BP NS can be quickly degraded to non-toxic phosphate and phosphite. Ag NPs are a kind of effective antibacterial agent without antibiotic resistance. But they are not so stable in solution as they are easily oxidized and aggregated. One

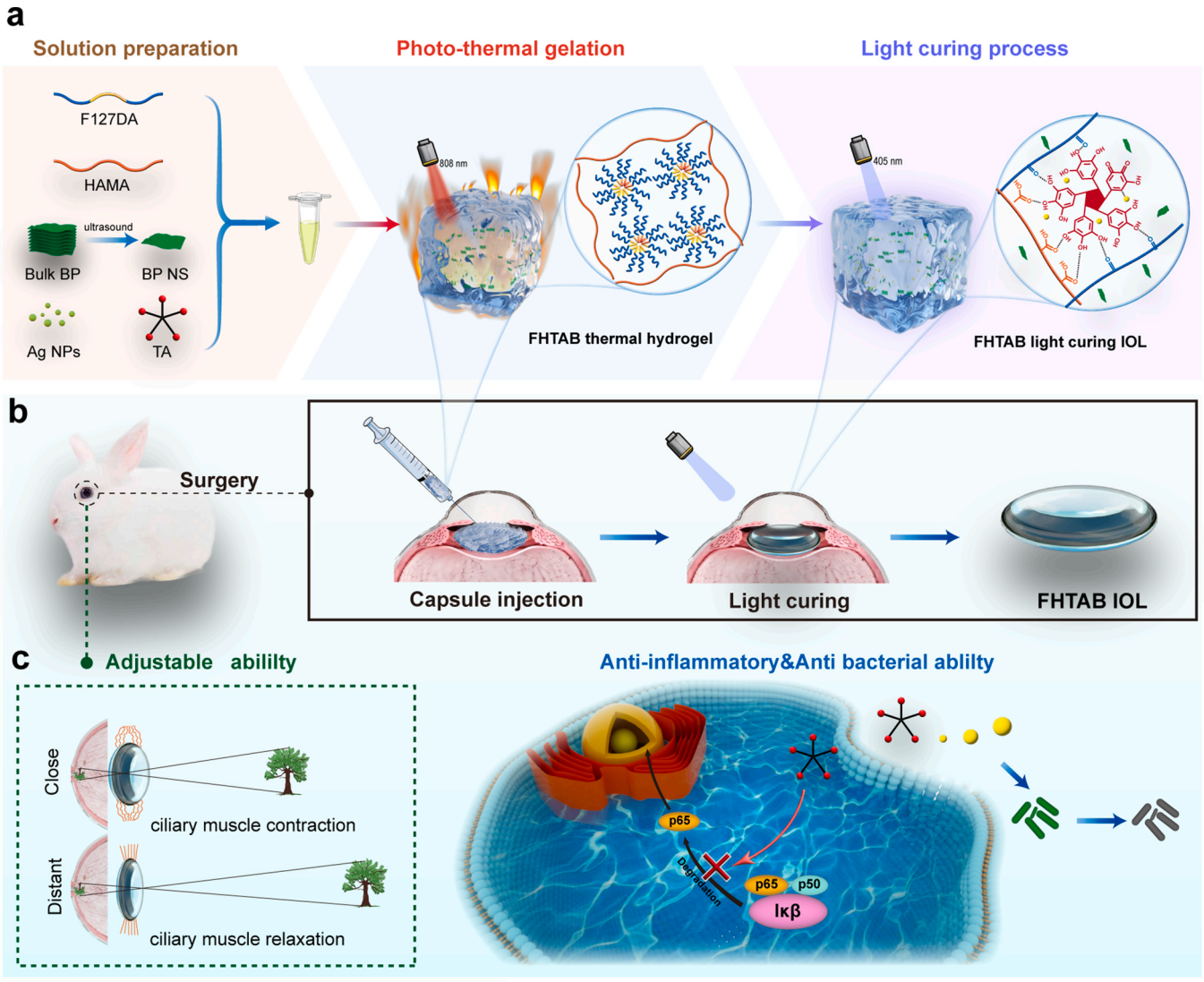

Scheme 1. Schematic illustration of FHTAB IOL. (a) The network structure of FHTAB hydrogel at different steps. (b)The process of injectable hydrogel-based FHTAB IOL prepared in capsular after cataract surgery. (c) The mechanism of adjustable ability, antibacterial and anti-inflammatory effect.

way to overcome this problem is to incorporate Ag NPs into biocompatible carriers such as hydrogels [29].

Based on the above concerns, this study designed and prepared a multifunctional injectable thermal-/photo-crosslinkable hydrogel as injectable, in situ curable and adjustable intraocular lens applications. The main composition of the injectable and adjustable IOL (FHTAB) is the F127DA and Hyaluronic acid Methacryloyl (HAMA) thermal-/photo-crosslinkable hydrogel, in which BP NS, TA, and Ag NPs were doped to give antibacterial, anti-inflammatory, and photothermal effect (Scheme 1). The use of BP NS allows FHTAB precursor fluid to undergo a rapid conformational transition to thermo-gelation under exposure to near infrared (NIR) light. After filling the empty capsular bag with FHTAB thermo-gelation, it can be rapidly cured to form an in situ photo-crosslinked intraocular lens under short-time blue light irradiation. The results indicate that such multifunctional FHTAB hydrogel could not only serve as an injectable, adjustable IOL but also has effective antibacterial and anti-inflammatory properties, which make it low complication occurrence after its intraocular implantation.

2. Experiment section

2.1. Materials and reagents

Black phosphorus (BP, bulk) was obtained from XFNANO Materials Tech Co. Ltd (Nanjing, China). N-methyl-2-pyrrolidinone (NMP), Tannic acid (TA), Ag nanoparticles (Ag NPs, 10–15 nm) were purchased from Aladdin Biochemical Technology Co. Polyether F127 Diacrylate (F127DA, $(PEO)_{99}$-$(PPO)_{67}$-$(PEO)_{99}$), Hyaluronic acid Methacryloyl (HAMA, 150 K) and photoinitiator lithium phenyl-2,4,6 trimethylbenzoyl phosphinate (LAP) were purchased from Engineering for Life (Suzhou, China). Phosphate-buffered saline (PBS) was purchased from Boster Biological Technology (Pleasanton, USA). Fetal bovine serum (FBS) and trypsin-ethylenediaminetetraacetic acid solution, penicillin-streptomycin solution, and Dulbecco's modified Eagle's medium/nutrient mixture F-12 (DMEM/F-12; 1:1 ratio) were purchased from Thermo Fisher Scientific (Carlsbad, USA). LIVE/DEAD™ BacLight™ bacterial viability assay kit was purchased from Thermofisher Co. 1,1-diphenyl-2-picrylhydrazine (DPPH) was purchased from APExBIO Co. 2′,7′-Dichlorodihydrofluorescein diacetate (DCFH-DA) was purchased from MedChemExpress Co. Lipopolysaccharide (LPS) was purchased from Sigma. DNA Damage Detection Kit, Annexin V-FITC Apoptosis Detection Kit, Calcein-AM&PI, p65 mouse monoclonal antibody, anti-mouse Cy3 and DAPI were purchased from Beyotime Co. Fast Pure Cell/Tissue Total RNA Isolation Kit, HI Script III All-in-one RT Super Mix Perfect for qPCR and Taq Pro Universal SYBR qPCR Master Mix Kit were purchased from Solarbio Co. All chemicals were of analytical grade and used following the manufacturers' instructions.

2.2. Cell experiments

Human lens epithelial cells (HLECs) and human corneal epithelial cells (HCECs) were bought from the Chinese Academy of Sciences Cell Bank (Shanghai, China), and were kept at 37 °C in a 5 % CO_2 humidified incubator. The DMEM media supplemented with 10 % FBS was used as the culture media.

2.2.1. Preparation and characterization of BP NS

BP NS (Black phosphorus nano sheet) was prepared by simple modified liquid exfoliation of bulk BP in NMP as reported [30,31]. In brief, 50 mg of bulk black phosphorus was dispersed in 100 mL NMP. The mixture was then ultrasonically treated on an ice bath for 6 h with a sonic tip (Amplifier: 50 %, On/Off cycle: 6 s/4 s). The NMP and ice bath were used to reduce the degradation of BP. The resulted brown suspension dispersion was subjected to centrifugation (1000 rpm, 15 min) for removal of un-exfoliated large BP. The supernatant was carefully collected and stored at 4 °C in a dark environment. Before use, the collected supernatant was centrifuged (10000 rpm, 15 min) to remove NMP and washed twice with ultrapure water.

The structure of BP NS was characterized by Raman spectra (HORIBA Scientific LabRAM HR Evolution) at 514 nm laser excitation. Transmission electron microscopy (TEM) was performed on JEOL JEM-F200 at an accelerating voltage of 200 kV. Dynamic light scattering (DLS) was measured and performed by Malvern Zetasizer Nano ZS90. BP NS was dispersed into ethanol solution by sonication, and then a few drops of the sample were added and dried on the mica sheet. Atomic force microscope (AFM) was photographed by Bruker Dimension Icon instrument. Absorbance was measured with Ultraviolet–visible (UV–vis) absorption spectrometer (UV-1780, Shimadzu). Before UV–vis measurements, the samples were sonicated to minimize the effect of the flakes restacking. The residual rate calculated from the absorbance represents the degradation of BP NS in water under different situations of merely in oxygenated/deoxygenated water or in both TA (200 μg/mL) and oxygenated water.

2.2.2. Fabrication of FHTAB IOL

TA and Ag NPs were first dissolved in 1 mL nitrogen degased PBS solution, then 2.5 mg LAP was added and sonicated for 30 min to gain homogeneous TA-Ag solution (TA: 200 μg/mL, Ag NPs: 5 ppm, LAP 0.25 % w/v). 210 mg F127DA and 10 mg HAMA powder were added and mixed for 12 h to harvest FHTA solution which contained F127DA: 21 % w/v, HAMA: 1 % w/v, and TA-Ag. BP NS was first washed and dried with a vacuum desiccator, and then added into FHTA solution with a concentration of 1 mg/mL and sonicated for 30 min to obtain FHTAB precursor liquid for hydrogels. In the lens mold, the photo-crosslinking process was carried out to obtain FHTAB IOL with 405 nm blue light.

2.2.3. Thermo-gelation and photo-curable properties of FHTAB

Prepared FHTAB precursor solution was taken into a glass vial at room temperature, and then incubated in a 37 °C water bath for 1 min. The glass vial was placed at an angle and photographed using a digital photograph. 0.2 mL of FHTAB precursor solution was aspirated into a syringe (needle size: 26 G) and then injected directly into water at a temperature of 37 °C. The injection procedure was recorded using the same method. The FHTAB precursor solution was placed on a transparent plastic plate. It was then exposed to 405 nm light (25 mW/cm^2) for 2 min and tilted at various angles (30° and 60°) to observe its photo-cured morphology and resistance to gravity.

2.2.4. Rheological measurements

The FHTAB was first moulded and placed in PBS to reach swelling equilibrium before being placed on the Kinexus Rheometer plate. Time sweeps were taken at a 0.1 % strain and 10 Hz frequency, with the temperature stabilized at 37 °C. Frequency sweeps were taken at a fixed 0.1 % strain with the frequency changing from 0.01 to 10 Hz. Throughout the rheological tests, the storage modulus (G') and viscous modulus (G") of hydrogel samples were recorded.

2.2.5. Morphological characterization

The FHTAB hydrogel morphology was studied using scanning electron microscopy (SEM). Before being observed, the freeze-dried samples were coated with a thin conductive layer of gold using a sputter coater. Then, the fracture surface morphology of hydrogels was examined using a ZEISS Sigma 300 (ZEISS, German). Afterward, the EDS-mapping was also operated with an accelerating voltage of 15 kV to determine the element distribution of C, O, Ag and P in FHTAB hydrogel.

2.2.6. Swelling behavior

The FHTAB hydrogel was photo-cured and freeze-dried. The freeze-dried and merely photo-cured samples were immersed in PBS at 37 °C. The hydrogel samples were weighed after wiping the excess water from their surface with dry filter paper when removed at a predetermined time point. The swelling rate of the hydrogel is calculated with the

following formula: The swelling rate (SR) is calculated as $[(M_t - M_o)/M_o] \times 100$ %, where M_t and M_o respectively represent the weight of the swollen hydrogel and the weight of the original hydrogel at time t.

2.2.7. In vitro degradation and release behavior of FHTAB

FHTAB hydrogel were submerged in PBS (pH = 7.4, 37 °C) at a shaking rate of 100 rpm. At predetermined time points, the samples were extracted and weighed after removing any excess water from their surfaces using dry filter paper. The weight ratio of the hydrogels was calculated using following formula: Degradation Rate (%) = $(W_o - W_t)/W_o \times 100$ %. Herein, W_t and W_o represent the weight of the remaining FHTAB hydrogel after degradation at different time points and the initial weight of the FHTAB hydrogel, respectively.

The release behavior analysis of FHTAB was also studied. Briefly, 500 μL FHTAB hydrogel was immersed in 2 mL PBS (pH = 7.4) at 37 °C with a shaking rate of 100 rpm. Then, 250 μL supernatant was collected at a predetermined period and replaced with 250 μL fresh buffer. FHAB (without TA) was operated with a similar method as a control. The Ag NPs and TA release profiles were obtained on a microplate reader.

2.2.8. Mechanical and optical properties of FHTAB IOL

Transparency of the FHTAB hydrogel cured by injection into the 3D printed IOL molds was generally observed with an HD camera. The compressive test was performed at 37 °C on an INSTRON 5982 test machine. A compression test was performed on cylindrical samples with a diameter of 10 mm and height of 4 mm at a displacement rate of 1 mm/min and stopped at 40 % strain. The UV–vis spectroscopy was deployed to quantify the alteration in transmittance from 300 nm to 800 nm, accompanied by a control sample thickness of 2 mm. The refractive index was measured by an Abbe refractometer (WYA-2WAJ, Japan). The resolution is determined by positioning the FHTAB at an optical resolution board (USAF 1951) and capturing an image of it. A colorimetric evaluation, according to the CIE L*a*b* system, was performed with the application of the FHTAB hydrogel via a colorimeter (LS173) and then graphed using the parameter lightness (L*), redness (a*) and yellowness (b*).

2.2.9. Photothermal property of FHTAB hydrogel

Photothermal property analysis was operated following previous method [32]. Briefly, 100 μL of FH, FHT, FHTA and FHTAB precursor solution were used to prepare hemispherical hydrogels. The real-time temperature and images were recorded with an infrared thermal camera (Fortic 225RD-L39C). Four types of hydrogels were exposed to an 808 nm light (1.0 W/cm^2) for 5 min. Afterward, FHTAB was under 808 nm light irradiation for 5 min with various power densities (0.5, 0.8, and 1.0 W/cm^2). Finally, FHTAB hydrogels containing different concentrations of BPNSs (0.25, 0.5, 1 mg/mL) were irradiated by 808 nm light (1.0 W/cm^2) for 5 min. The gel morphology and injectable behavior of FHTAB hydrogel precursor fluid were also examined after photothermal behavior.

2.2.10. Antibacterial properties of FHTAB

To evaluate the antibacterial activity of the hydrogels, *E. coli* (ATCC 35218) and *S. aureus* (ATCC 25923) were used. The inhibition zone method was used to evaluate the antibacterial activity of each sample group. Specifically, bacterial suspensions (100 μL, 1×10^4 CFU/mL) were spread on the nutrient agar plate and then the samples were gently placed on it. Finally, the inhibition zone was photographed with a digital camera after 12 h incubation at 37 °C. Then, 100 μL bacterial suspension of 1×10^5 CFU/mL was prepared and this solution was added to the hydrogel surface (100 μL). The substrate was placed in a 96-well culture plate and incubated at 37 °C for 24 h. Afterward, 100 μL of sterilized PBS was added to each well to resuspend any bacterial survivors. Finally, 50 μL of the samples from different groups were incubated on agar plates at 37 °C for 24 h, and the number of colony-forming units was recorded promptly. In the meantime, the LIVE/DEAD™ BacLight™ bacterial viability assay kit was also used to evaluate the antibacterial ability of FHTAB hydrogel.

2.2.11. Antioxidant efficiency of the FHTAB

The free radical scavenging ability of the hydrogels was evaluated by DPPH. To perform the assay, 0.5 mL of freshly prepared DPPH ethanol solution (0.5 mM) was mixed with 1.5 mL materials in ethanol solution (containing 100 μL FHTAB hydrogel) and incubated for 30 min under light-avoiding conditions. The mixture merely had DPPH and ethanol was as control. Then, the mixture solution was detected with UV–vis spectrometer and placed in a 96-well plate to measure absorbance at 517 nm. Upon completion of the incubation period, the formula was utilized to evaluate the DPPH free radical scavenging effect: $DPPH_{Scavenging\ effect}$ (%) = $(1 - OD_{sample}/OD_{control}) \times 100$ %.

To further examine its antioxidant capacity, DCFH-DA was used to investigate the intracellular ROS scavenging abilities of FHTAB hydrogel. Briefly, HLECs were seeded in each well of 96-well plate with a concentration of 1×10^4 cells/well. FH, FHT, and FHTAB hydrogels (40 μL) were respectively added into three groups well. The cells were then treated with DMEM solution containing 0.4 mM H_2O_2 for 2 h. After that, the hydrogels and H_2O_2 contained DMEM solution were removed and the cells were washed with PBS 3 times. Then, the DCFH-DA probe was added and incubated for 20 min and the images were captured by a fluorescence microscope.

2.2.12. In vitro anti-inflammatory capacity of FHTAB

The FHTAB hydrogel was co-cultured with RAW 264.7 cells, which were activated to produce an inflammatory behavior with LPS, and the levels of three inflammatory factors were measured by enzyme-linked immunosorbent assay (ELISA). In brief, RAW 264.7 cells were cultured in 24-well plates at a density of 1×10^5 cells/well. After overnight incubation, the liquid was aspirated and replaced with fresh DMEM and 100 μL of FHTAB hydrogel. The cells were then incubated for 3 h. All groups except the negative control group were given 10 μL of LPS solution to achieve a final concentration of 1 μg/mL. The samples were then incubated and the liquid in the well plates was transferred to 1.5 mL EP tubes and centrifuged for 10 min at (4 °C, 12000 rpm). Supernatants were assayed for TNF-α, IL-6, and IL-1β inflammatory factor levels using ELISA kits.

RT-qPCR experiments were also performed to detect mRNA expression levels of inflammatory factors. Briefly, total RNA was extracted from RAW 264.7 cells according to the steps of the Fast Pure Cell/Tissue Total RNA Isolation Kit. Subsequently, reverse transcription was performed according to the steps of HI Script III All-in-one RT Super Mix Perfect for qPCR to obtain cDNA. Finally, the cDNA was analyzed by real-time fluorescence quantitative analysis in a PCR instrument (Q5) following the steps of Taq Pro Universal SYBR qPCR Master Mix. The primer sequences used can be found in Supplementary Materials (Table S1).

2.2.13. Mechanism of anti-inflammatory effects from FHTAB IOL

NF-κB is a classical pathway of inflammation, regulated by p65. The study examined the expression and nuclear translocation of p65, a major subunit of NF-κB, in RAW 264.7 macrophages through cellular immunofluorescence after co-culture with FHTAB. Briefly, unpolarized RAW 264.7 was planted on the surface of cell crawls with a planting density of 2×10^4 cells/well, and incubated overnight in a cell incubator after adding FHTAB hydrogel. After fixation and sealing, NF-κB p65 mouse monoclonal antibody was added and incubated for 1 h at room temperature. Anti-mouse Cy3 was added and incubated for 1 h at room temperature. DAPI was added and staining was carried out for 5 min at room temperature. The slices were sealed and observed under a laser confocal fluorescence microscope.

2.2.14. Biocompatibility evaluation of FHTAB IOL

The phototoxicity of blue light (405 nm) to HCECs was assessed by

detecting DNA damage (γ-H2AX immunofluorescence assay) following a specific duration of irradiation. For cytocompatibility, the hydrogels were prepared in the cell culture plate and washed 3 times with PBS solution. Then, HLECs were inoculated on the surface of hydrogel with a density of 5000 cells/well. After 1 day' incubation, live and dead assay was used to test the cell viability by staining the cells with hydrogel contact. Hydrogel extracts were also used to evaluate hydrogel cytocompatibility. After hydrogel formation, the hydrogels were submerged in DMEM comprising 10 % FBS and 1 % penicillin/streptomycin. It was incubated at 37 °C for 3 d. HLECs were inoculated in a 96-well cell culture plate with a density of 10000 cells/well. The culture medium was then replaced with hydrogel extracts after the cells had attached to the surface. After 1 day' incubation, the cell viability was assessed with CCK-8 and Annexin V-FITC/PI flow cytometry.

2.2.15. *In vivo efficiency of FHTAB IOL*

The right eyes of 2-month-old New Zealand white rabbits were selected to implant the FHTAB IOL after cataract surgery by phacoemulsification. In brief, the hydrogel precursor solution of FHTAB first underwent initial sterilization through a 0.22 μm filter membrane. Subsequently, NIR light irradiation for 3 min was used to achieve the thermal gelation transformation. Animal eyes with clean empty lens capsular bags were obtained at the end of phacoemulsification. Then, the thermo-gelled FHTAB hydrogel was injected into the empty capsular bag and rapidly irradiated with 405 nm blue light for 30 s for intraocular light curing process.

Postoperative observations were conducted using slit-lamp microscopy, anterior segment optical coherence tomography (AS-OCT), along with monitoring of intraocular pressure (IOP) and body weight in the first week. The levels of inflammatory factors in the aqueous humor of three groups: nonsurgical control group, surgery-only group, and FHTAB IOL implantation group (FHTAB) were measured at 3 d postoperatively using an ELISA kit. Additionally, the expression of IL-6 in the iris of the dissected intraocular tissues was analyzed by tissue immunofluorescence staining. Frozen sections of iris tissue were incubated overnight with diluted IL-6 primary antibody, followed by incubation with 455 fluorescent secondary antibody. Nuclear staining was performed with DAPI. The sections were then examined under a confocal microscope. Also, the electroretinogram exam (ERG) was operated to evaluate the biocompatibility and safety after FHTAB IOL implantation. The experimental animals were finally euthanized and underwent ocular autopsy, and specific tissues were isolated and stained for hematoxylin and eosin (H&E) analysis.

2.3. *Statistical analysis*

All data were expressed as mean ± SD (standard deviation) from at least three independent experiments. Statistically significant, one-way ANOVA analysis was used; $p < 0.05$ (*), $p < 0.01$ (**), or $p < 0.001$ (***) are marked in the figures.

3. Results and discussion

3.1. *Characterization and degradation of BP NS*

Few-layer BP NS was prepared by simple modified liquid exfoliation in NMP. Raman spectra (Fig. 1a) and TEM analysis (Fig. 1b) indicated that the BP structure was preserved after liquid exfoliation and exhibited as few-layer sheets. The BP NS suspension was pale gray after twice washing with water with its average size around 150 nm (Fig. 1c) and average thickness around 2 nm (Fig. 1d), which were measured by DLS and AFM, respectively. As shown in UV–vis absorption spectrum, the characteristic absorption peak of BP NS was at 475 nm, and the concentration of prepared BP NS suspension was about 4 mg/mL. To study its degradability, diluted BP NS was placed in various aqueous environments (light, 37 °C), including merely in oxygenated/deoxygenated water (without TA) or oxygenated water (with TA 200 μg/mL). As shown in Fig. 1e, the absorbance of BP NS suspension was decreased with storage time in all three aqueous environments, which indicated the degradation of BP NS. The degradation of the BP NS in the deoxygenated water was slightly better than that in the oxygenated water, but both of them were degraded over 50 % within 2 d. However, BP NS was well able to prevent its oxidation when it was in the TA contained aqueous solution. Nearly half of the BP NS in oxygenated water containing TA was still retained even after 7 days, whereas it was just around 16 % in the TA free water in either oxygenated or deoxygenated states (Fig. 1f). Therefore, TA could prevent the rapid degradation of BP NS by antioxidant function even in oxygenated aqueous solutions and bright environments.

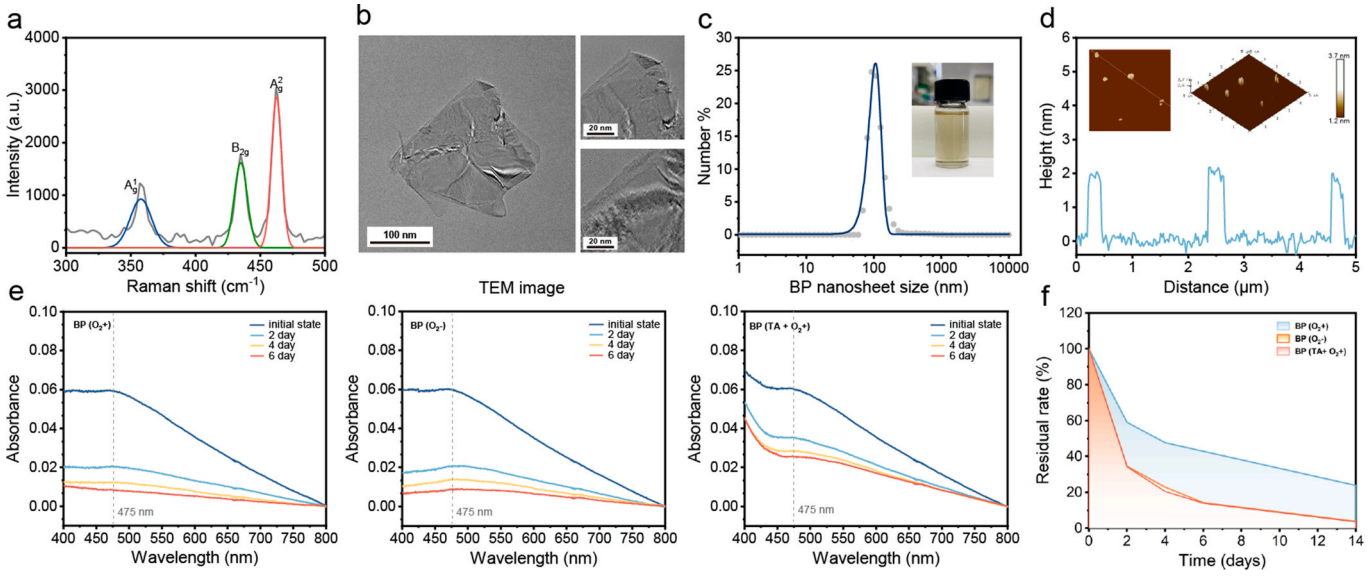

Fig. 1. Characterization and degradation of BP NS. (a) Raman spectra of BP NS suspension. (b) Different magnifications of TEM image of BP NS (Scale bar = 100 nm and 20 nm). (c) Size distribution of BP NS in water measured by DLS. (d) AFM image and thickness of BP NS. (e) UV–vis spectra of BP in water with different treatments (merely oxygenated or deoxygenated water, both TA and oxygenated water). (f) Normalized residual rate of BP NS during 14 d.

3.2. Preparation and characterization of FHTAB hydrogel

To develop an adjustable lens suitable for intraocular capsular bag implantation and in situ molding, FHTAB IOL was prepared and injected as Scheme 1. As shown in Fig. 2a, all of the FH, FHTA, and FHTAB precursor liquids were high flow liquids at room temperature around 20 °C. When tilted, all three liquids in the bottle swiftly reached the horizontal position due to the force of gravity. However, when incubated in 37 °C water bath for 10 s, the hydrogel precursor liquid in the bottle increased in viscosity and showed a greater inclination to the horizontal when placed with the same angle of tilt and time of placement. Afterward, the hydrogel precursor liquid was drawn into a syringe (room temperature) and then directly injected into PBS solution (37 °C). All precursor liquid could be injected effortlessly and exhibited rapid thermo-gelation behavior when injected into 37 °C PBS solution. This was because of the PEO-PPO-PEO triblock copolymers structure of F127DA in FH, FHTA, and FHTAB, which was self-assembled to form micelles when exceeding critical micelle temperature.

The hydrogel precursor liquid was then injected into a transparent circular mold and irradiated under 405 nm light for 2 min. FH is transparent and colorless, whereas FHTA and FHTAB exhibit a pale yellow and yellowish-brown hue, respectively, owing to the presence of silver nanoparticles and BP NS (Fig. 2b). Compared with PBS, FH, FHTA, and FHTAB were all rapidly photo-curried and they adhered to the surface against gravity, when the mold was tilted at 30° and 60°. Then, the general observation of photo-curable FHTAB hydrogel under compression and stretching was detected. As shown in Fig. 2c and d, FHTAB hydrogel could withstand large deformation (Video 1). On the other hand, the shear storage moduli (G′) and loss moduli (G″) were recorded by rheometer. FHTAB hydrogel underwent a rapid photo-curing process during 30 s with 405 nm light (Fig. 2e). In addition, the G′ of FHTAB increased significantly with the extension of exposure time. After 20 s' irradiation, the G' of FHTAB hydrogel increased smaller and remained relatively stable after light irradiation for 30 s. According to the above results, FHTAB had rapid thermo-gelation and photo-curing properties.

Supplementary video related to this article can be found at https://doi.org/10.1016/j.bioactmat.2024.07.005

3.3. Physical properties characterization

SEM was used to analyze the morphology of the multifunctional hydrogels. It can be seen in Fig. 3a that the photo-crosslinked FHTAB hydrogel has a pore structure with pore sizes ranging from 3 μm to 5 μm. Both interior and surface exhibited a dense and uniform network structure, which may be due to the hydrogen bond between TA and F127D and HAMA. Dispersed BP NS can also be observed inside and on the surface of the FHTAB. The EDS-mapping was then operated to analyze the distribution of components in FHTAB. As shown in Fig. 3b, BP NS and Ag NP's distinctive elements P and Ag were uniformly dispersed in the FHTAB.

The water uptake capacity was measured to determine the hydrogel swelling properties of the prepared FHTAB hydrogel. The FHTAB hydrogel's swelling rate was monitored for 8 h at 37 °C in PBS. As shown in Fig. 3c, the swelling rate of FHTAB freeze-dried and FHTAB hydrogel samples gradually increased within 2 h incubation and then tended to be stable. The maximum swelling rate of freeze-dried FHTAB was around 640 % and of wet FHTAB hydrogel was approximately 14 %.

The degradation of FHTAB IOL in liquids is also of great significance. FHTAB and F127DA were prepared and immersed in PBS at 37 °C, weighing the remaining mass at pre-determined time intervals. After 11 d, 7.69 ± 1.47 % weight loss of FHTAB hydrogels was observed, and the F127DA hydrogel reduced 8.23 ± 1.23 %. Then, the degradation curve reaches a plateau, with the degradation ratio around 9.8 % at the 50 d (Fig. 3d).

3.4. In vitro release of Ag NPs and TA

The release of Ag NPs depended on the pore size, the degradation degree of the hydrogel and the structure of the hydrogel. The cumulative release curves of Ag NPs and TA from hydrogel were calculated within 14 d. As shown in Fig. 3e, when the phenolic hydroxyl group of TA formed a hydrogen bond with F127DA and HAMA, TA was immobilized in the hydrogel and the release was limited, it was released slowly after 4 h and with a cumulative release of 44 % at 3 d. The Ag NPs in FHAB hydrogel (without TA) had an initial burst release of about 92 % at 12 h, and almost released all at 1 d. While the Ag NPs in FHTAB hydrogel (contain TA) exhibited a gentle curve with a release of 90 % at 3 d, which might be due to the electron transfer between Ag NPs and TA which formed local metal–phenolic networks.

3.5. Lens characterization analysis

The mechanical property and optical properties of FHTAB IOL play a crucial role in their capacity to substitute natural ocular lens in the capsular bag. As exhibited in Fig. 4a, FHTAB was firstly injected into ring textured 3D printed IOL molds. After photo-curing process, FHTAB hydrogel could be easily pickup and the ring texture was also clearly

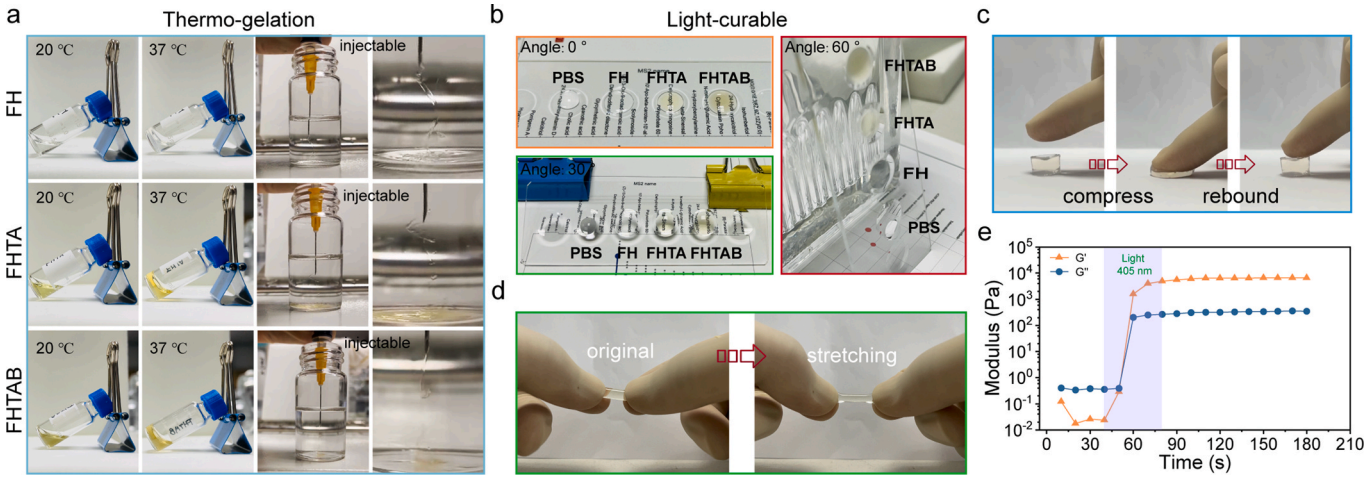

Fig. 2. Characterization of FHTAB hydrogel. (a) The thermos-gelation process photographs of FH, FHTA and FHTAB. (b) The images of FH, FHTA and FHTAB after photo-curing process and its ability in against gravity at different placement angles. (c, d) Compressive and stretching performance of FHTAB. (e) Modulus change during photo-curing process with 405 nm light.

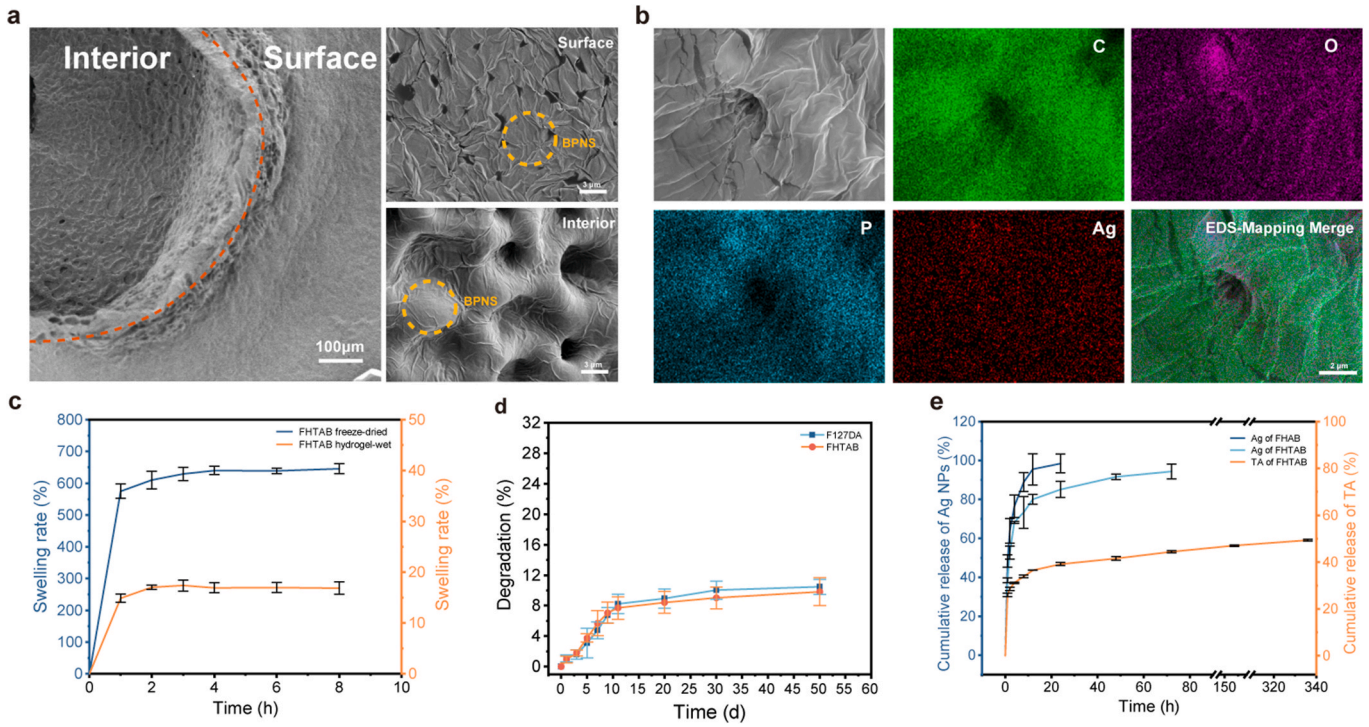

Fig. 3. Characterization of photo-cured FHTAB hydrogel. (a) SEM images of FHTAB. (b) EDS-mapping and element distribution of C, O, P, Ag. (c) Swelling properties of FHTAB. (d) The degradation rate of hydrogels in PBS. (e) TA and Ag release of FHTA and FHTAB in PBS.

visible on the hydrogel, which indicated that FHTAB had a good shape adaptation. Then, compression tests were performed to study the mechanical properties of FHTAB IOL. The maximum compressive strain was set to 40 %, which was similar to natural lens adjustment (Fig. 4b). According to the force-time-compressive strain curves, the force required to reach the maximum compressive strain was only about 1.5 N. Then, multiple compression-rebound processes were operated to simulate the changes in the shape of the natural lens of the human when looking at far and near. After undergoing three cycles, FHTAB IOL demonstrated outstanding compression properties, demonstrating its adaptability.

Transmittance, a crucial optical characteristic of the IOL, was also evaluated. The transmittance of FHTAB IOL was about 92 %, which was close to the transmittance of natural rabbit eye lens. Moreover, the transmittance of FHTAB IOL raised to 94 % after being immersed in saline at 37 °C for 10 d. This was due to the degradation of BP NS in FHTAB IOL.

The refractive index of natural rabbit lens, commercial IOLs, and FHTAB IOL was 1.38, 1.43, and 1.365, respectively (Fig. 4d). FHTAB IOL were found closer to natural lens. Compared with FH IOL, refractive index of FHTAB IOL raised 0.002, which indicated that the refractive index could be increased by increasing the solute in the hydrogel.

Providing good resolution is also one of the important roles of the lens. The resolutions of the fabricated injectable IOLs were detected by the resolution plates. As exhibited in Fig. 4e, commercial IOLs provided 161 mm/lp resolution, FH IOL provided 152.5 mm/lp and FHTA IOL provided 161 mm/lp. However, the resolution of the FHTAB IOL with the addition of BP NS was 128 mm/lp. This result indicated that BP NSs will affect the resolution to some extent. Notably, the resolution of FHTA was always superior to the FH after repeating with multiple tests. This is due to the yellowish color of the FHTA IOL loaded with Ag NPs, which impedes a certain degree of short-wave blue-violet light (400 nm–500 nm) and reduces its scattering in ocular to form glare that improves contrast sensitivity [33].

Color is a pervasive feature of psychological experience, having a vital role in many aspects of human mind and behavior, such as basic vision, scene perception, and object recognition [34]. CIE Lab is a color system that describes human visual perception digitally, based on physiological principles [35,36]. Green color (L: 51.79, a: −49.19, b: 21.48, C: 53.67, h: 156.4) was selected as the standard color palette, and the color differences occurring after the light through the FHTAB IOL or commercial IOLs were identified via a colorimeter. As exhibited in Fig. 4f, the most discriminable change of commercial IOLs was found in color along the a*-axis (redness) in CIE Lab color space, followed by the b*-axis (yellowness). Moreover, the total color aberration (ΔE*ab) of FHTAB IOL (ΔE*ab = 3.3) was much smaller than the commercial IOLs (ΔE*ab = 16), compared with the standard color.

3.6. Photothermal performance of FHTAB hydrogel

In addition to providing attachment points for TA in the FHTAB hydrogel, BP NS also endowed it with a good photothermal effect. Due to the photothermal effect of BP induced by 808 nm light, the hydrogel showed a sensitivity to 808 nm light. The changes in temperature of the FHTAB hydrogel upon 808 nm light irradiation could be tracked with an IR thermal camera at a distance of 7.5 cm from the hydrogel and light (Fig. 5a). Fig. 5b showed that temperature of hydrogels without BP NS (FH, FHT and FHTA) were almost unchanged after irradiation for 300 s. In contrast, the BP NS loaded hydrogels (FHTAB) have a significant photothermal effect. As the intensity of 808 nm light increased, the FHTAB could reach a higher temperature of 52 °C when the power was 1.0 W/cm^2 (Fig. 5c). Fig. 5d showed the corresponding IR thermal images of the FHTAB hydrogel with different BP NS contents. The temperature of FHTAB with a BP NS content of 750 μg/mL increased from 22 to 31 °C when exposed to the light for 300 s, and the maximum temperature increased with the BP NS content increasing.

At the same time, the thermal gelation process via photothermal effect was also investigated. To enable easier observation, little red pigment was mixed with the hydrogel. The FHTAB hydrogel precursor liquid was prepared at about 13 °C and showed a flowable liquid state. Its temperature rose to about 45 °C when exposed to light for 3 min, and it clearly showed a gelation state (Fig. 5e). In this state, it was injected

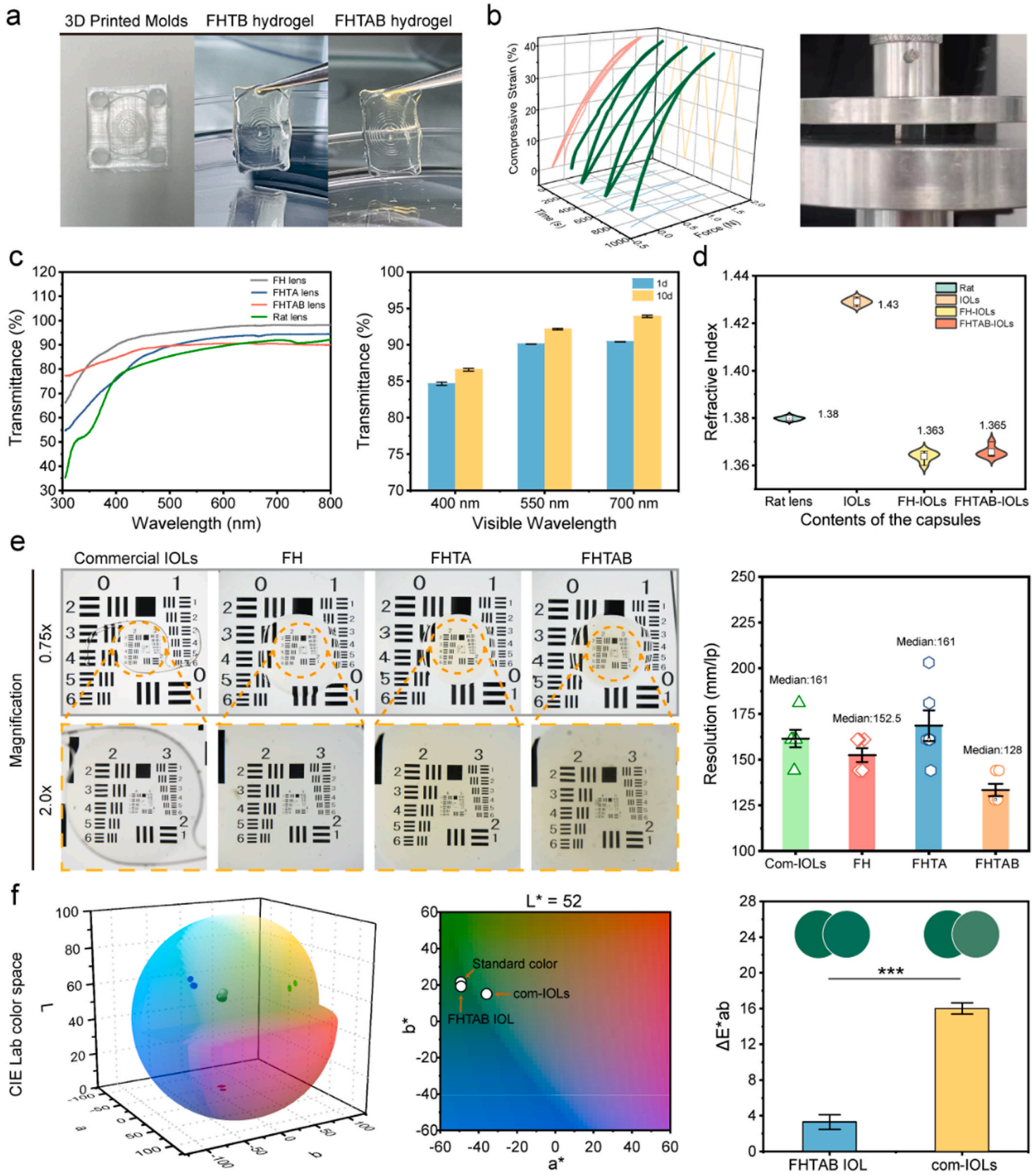

Fig. 4. The optical properties of FHTAB IOL. (a) Images of photo-cured hydrogels through a 3D printed IOL mold. (b) Images of compression testing and the Force-Compressive strain-time curves for FHTAB IOL under 3 cycles. (c) Transmittance of hydrogels at 1 d and 10 d immersing in a saline solution. (d) Transmittance of IOL compared with rabbit lens content and commercial IOLs. (e) Resolution of FHTAB IOL compared to commercial IOLs. (f) Color aberration of FHTAB IOL through CIE Lab color space analysis.

into saline at a temperature of 37 °C through needles of different sizes to simulate the behavior of an anterior chamber injection. Compared with the results in Fig. 2a, pre-photo heating for 3 min before injection showed much better gelation properties (Fig. 5e–Video 2). The reason for this difference was that temperature caused structural transformation still required time. The time of short injection process was not sufficient for the complete thermo-gelation of the FHTAB precursor liquid. Therefore, pre-heating in vitro with NIR light would be more

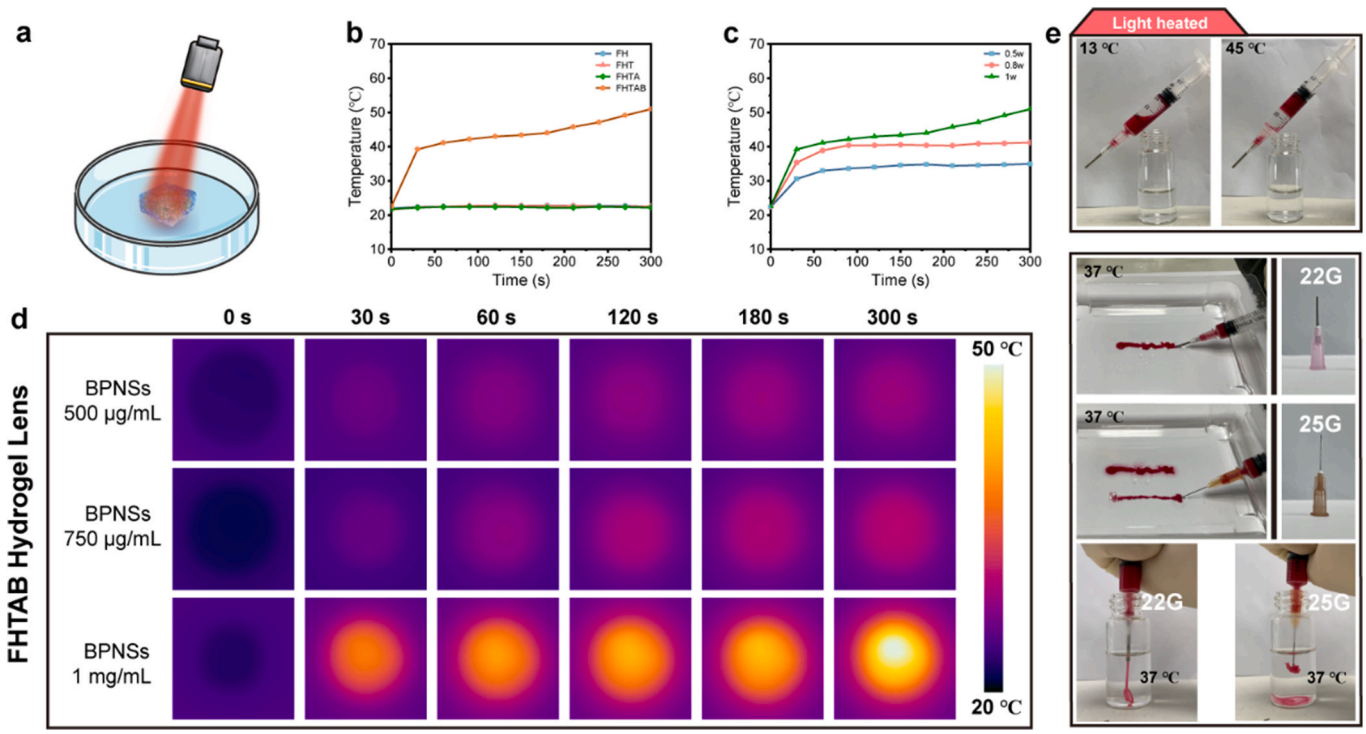

Fig. 5. Photothermal property of FHTAB hydrogel. (a)Schematic of the temperature rise of the composite hydrogel under 808 nm light. (b) Photothermal behavior of FH, FHT, FHTA and FHTAB. (c) Heat generation capability of FHTAB under various 808 nm light powers. (d) The corresponding IR thermal images of FHTAB hydrogel with a concentration of BP NS from 500 μg/mL to 1 mg/mL. (e) Thermo-gelation by photothermal effect and injection process of FHTAB through different needle sizes.

effective for practical applications.

Supplementary video related to this article can be found at https://doi.org/10.1016/j.bioactmat.2024.07.005

3.7. Antibacterial ability of the FHTAB hydrogel

S. aureus and *E. coli* were used as representative bacteria in infection to evaluate the antibacterial properties of the FHTAB hydrogels in vitro. After the co-incubation with FH, FHTB and FHTAB hydrogels for 24 h, the results of antibacterial activity were exhibited in Fig. 6a and b. Compared with the FH hydrogel, the numbers of bacterial colony-forming units (CFU) were reduced to 94 % ± 2.90 % for *S. aureus* and 88 % ± 1.42 % for *E. coli* with the addition of TA (FHTB group). In addition, when adding with Ag NPs (5 ppm), the FHTAB group exhibited much better antibacterial properties with the antibacterial ratio increased to nearly 100 %. The bacteria were seeded on the surface of hydrogel, and then stained with a LIVE/DEAD™ BacLight™ bacterial Staining kit. As illustrated in Fig. 6c, the pure FH hydrogel exhibited minimal lived bacterial retention following staining, which indicated that FH hydrogels had some resistance to adhesion. When added with TA and Ag NPs, the dead bacteria were detected, which exhibited the antibacterial capacity of FHTAB hydrogel. Bactericidal effects based on the photothermal effect have also been studied. As a complement to this, similar antimicrobial experiments were carried out with *P. aeruginosa* as a common bacterium in intraocular infections. As shown in Fig. S1, FHTAB also has strong antibacterial activity against *P. aeruginosa*. As exhibited in Fig. 6d, disc-shaped FHTAB hydrogels were placed on well plates pre-cultured with *S. aureus* (2×10^6 CFU). Merely 5 min contact without NIR irradiation did not produce obvious antibacterial effect, which was exhibited as the green area. After FHTAB hydrogel was exposed to NIR light for 3 min, the FHTAB was heated and the heat-killed bacteria were found beneath the FHTAB hydrogel, which showed as a red area.

3.8. FHTAB hydrogel scavenges ROS

As secondary messengers, ROS have a substantial influence on wound healing response after cataract surgery, which induces the EMT process when the HLECs are constantly exposed to oxidative stress. The anti-oxidative property was initially assessed through the DPPH radical scavenging assay, which is an in vitro stabilized free radical and decreases in absorbance after being scavenged. As shown in Fig. 7a, the hydrogel without TA exhibited quite weak ROS scavenging capacity, but the scavenging ability of FHTB and FHTAB hydrogels was obvious and similar. The FHB hydrogel cleared about 10 %, while FHTB and FHTAB hydrogel cleared about 65 % and 61 %, respectively (Fig. 7b). These results demonstrated that the FHTAB hydrogel had significant antioxidant properties, and its effects were mainly derived from TA.

DCFH-DA assay was further examined to evaluate the ROS scavenging capacity on the cellular level. As ROS oxidizes DCFH into DCF, it emits green fluorescence, which can be used to estimate the remaining ROS. Fluorescent images in Fig. 7d revealed that the remaining ROS level in FHB group was similar to the positive group when treated with H_2O_2. The group containing TA (FHTB and FHTAB group) exhibited comparable ROS scavenging capacity to negative control. The semi-quantitative results in Fig. 7c also confirmed this.

3.9. FHTAB hydrogel attenuates inflammation

An in vitro inflammatory cell model was constructed using LPS-inducible RAW 264.7 cells. The levels of downstream inflammatory factors TNF-α, IL-6, and IL-1β were detected using ELISA kits after co-culturing with FH and FHTAB. Fig. 7e showed that the levels of all relevant inflammatory factors significantly increased after LPS stimulation. Co-culture with FH resulted in a significant decrease in TNF-α and IL-1β levels, but no significant expression changes in IL-6 were observed. Co-culture with FHTAB resulted in varying degrees of decrease in TNF-α, IL-6, and IL-1β levels.

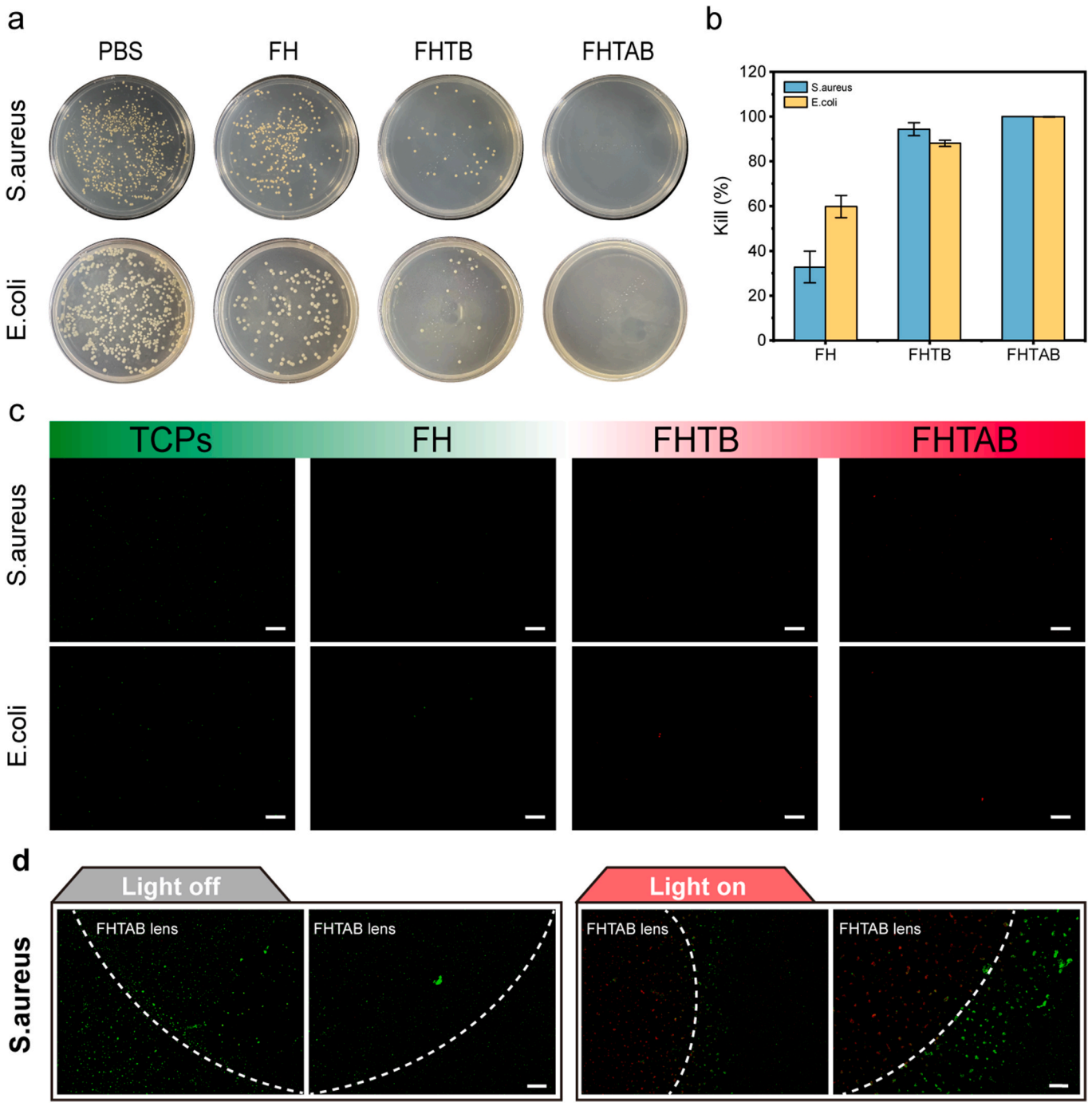

Fig. 6. Determination of antibacterial capacity of FHTAB hydrogel. (a) Pictures of each group spread on an agar plate after the FH, FHTB and FHTAB co-incubated with *S. aureus* and *E. coli* bacterial suspensions. (b) Killing rate of *E. coli* and *S. aureus* in each group. (c) Representative live/dead staining images of *S. aureus* and *E. coli* bacteria cultured on FH, FHTB and THTAB hydrogel (scale bar = 100 μm). (d) Sterilization of FHTAB lens after exposure to 808 nm light for 3 min.

The gene expression levels of the relevant inflammatory factors were analyzed using RT-qPCR. Fig. 7f showed that LPS induction significantly elevated the mRNA levels of TNF-α, IL-6, and IL-1β. However, after co-culture with FHTAB, the levels of these inflammatory factors decreased. This indicated that the TA released from FHTAB effectively inhibited transcription, which was also consistent with the ELISA results.

3.10. *FHTAB IOL suppresses inflammation through NF-κb*

NF-κB is a classical pathway of inflammation. p65 regulates this signaling pathway and plays a crucial role in activating the inflammatory response. It mainly regulates the transcriptional process by modulating the phosphorylation and nuclear translocation of p65. To detect the expression and nuclear translocation, cell immunofluorescence staining was performed after the co-incubation of RAW 264.7 with FHTAB. As shown in Fig. 8a, under normal conditions (Control group), p65 was concentrated in the cytoplasm. If stimulated by LPS, the cells showed altered polarization and a significant increase in p65 entry into the nucleus. Similar results were observed in the FH group. However, in the FHTAB group, a significant decrease in p65 entry into the nucleus was observed, and the cells were not polarized. These findings indicate that FHTAB may have anti-inflammatory properties by inhibiting the

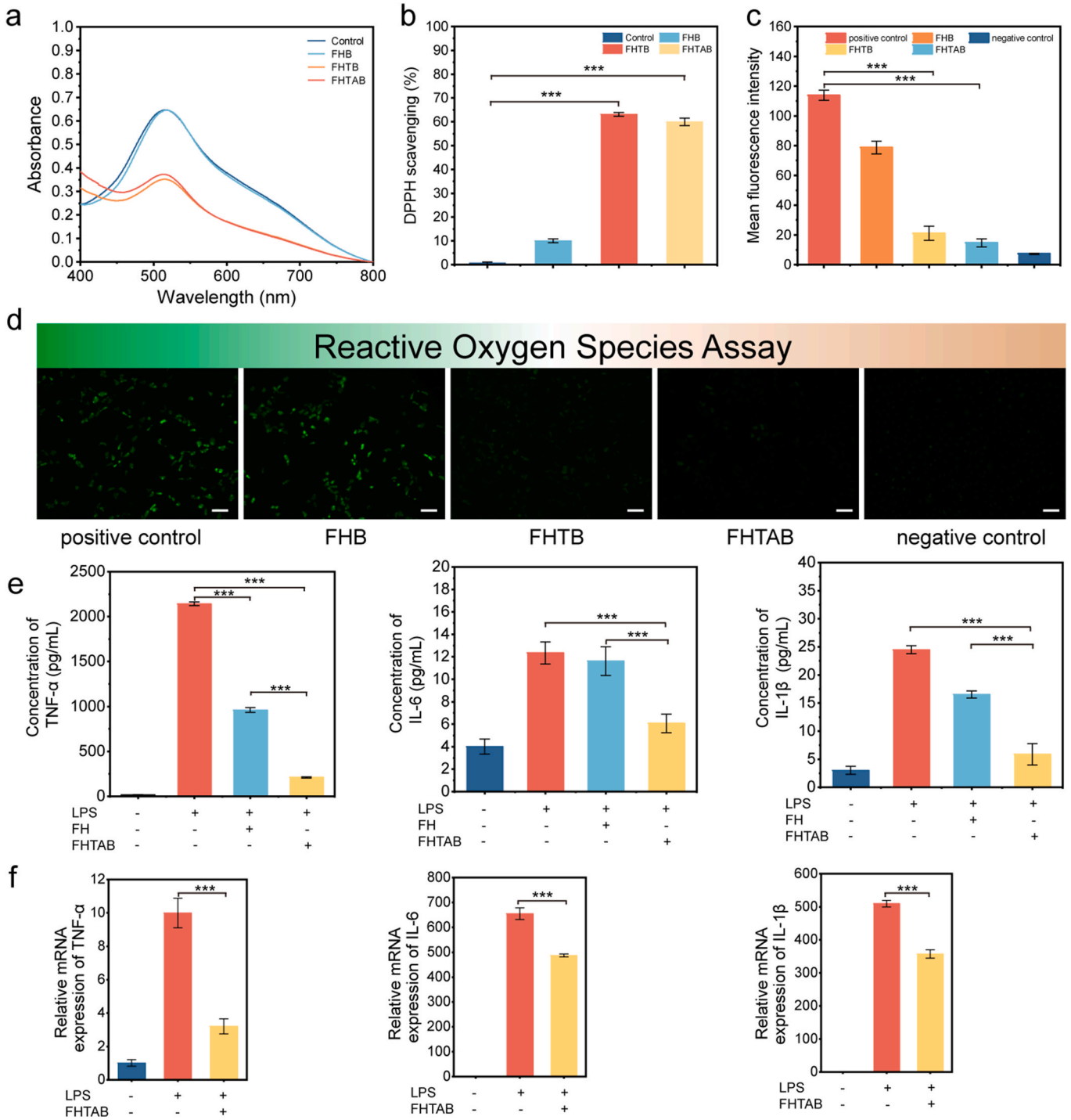

Fig. 7. Antioxidant capacity of FHTAB hydrogel. (a) The UV–vis spectrum of DPPH after being treated with FH, FHTB and FHTAB. (b) DPPH free radical scavenging assay results of FHTAB hydrogel. (c) Quantification of fluorescence intensity in the HLECs treated with H_2O_2 and FHTAB hydrogel. (d) DCFH-DA staining to detect ROS in cells. Scale bar = 100 μm. (e) Levels of inflammatory factors were determined by ELISA after incubation with FH, FHTB, and FHTAB. (f) Suppression of inflammatory factors at mRNA level after incubation with FHTAB was determined by RT-qPCR.

NF-κB pathway and decreasing the levels of inflammatory factors.

The impact of oxidative stress and inflammation on the proliferation of HLECs has been observed. The study investigated the effectiveness of FHTAB hydrogel IOL in reducing oxidative stress and inflammation. The results were analyzed by alarm blue. Fig. 8b showed that the proliferation level significantly increased after HLECs were stimulated by low concentrations of H_2O_2 or LPS. However, the proliferation level of cells was significantly inhibited after co-culture with FHTAB, which was similar to the normal level. This suggested that FHTAB could inhibit the elevated proliferation level of cells from oxidative stress or inflammation.

3.11. *In vitro biocompatibility evaluation of FHTAB IOL*

Cytocompatibility in construction and after FHTAB lens implantation is essential for clinical applications. Before forming, FHTAB IOL must be photo-cured with 405 nm blue-violet light. A previous study found that the cornea absorbed 63.56 % of ultraviolet (UV) light that

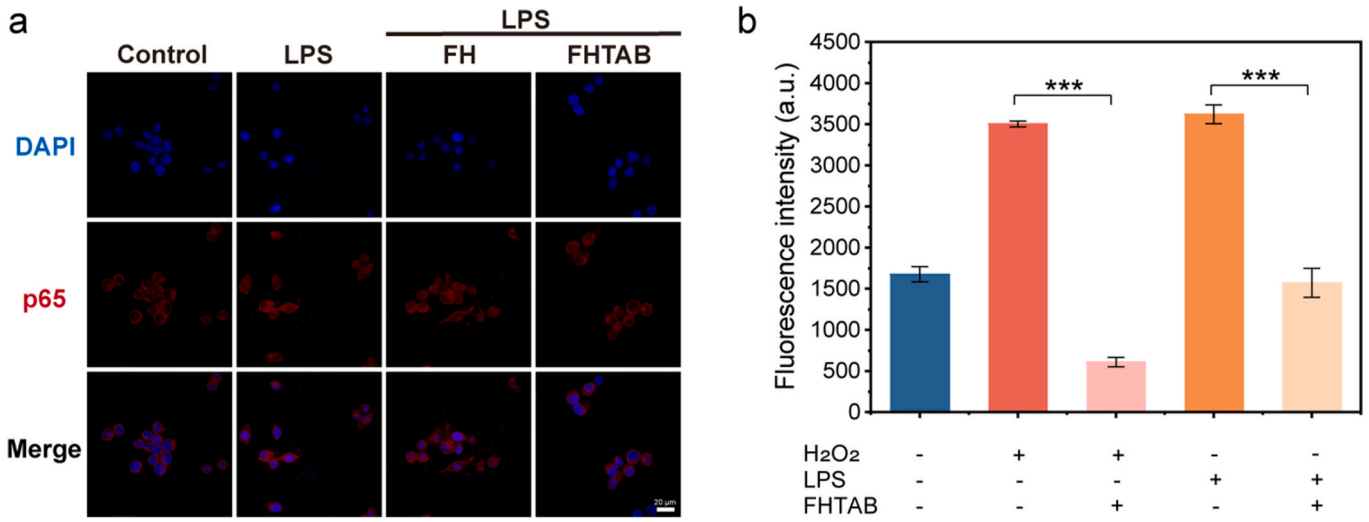

Fig. 8. Mechanism of anti-inflammatory from FHTAB IOL (a) Analysis of p65 nuclear translocation of NF-κB by immunofluorescence staining. (b) FHTAB hydrogel IOL reduced the cell proliferation level through anti-oxidant and anti-inflammatory effects.

reached the eye [37]. Compared with 365 nm ultraviolet-A (UVA) light, 405 nm light increases corneal penetration while still maintaining high energy, which brings a potential risk of cornea damage, especially with prolonged exposure. This damage usually manifests as damage to cellular DNA. Cellular DNA damage of HCECs was measured by detecting the amount of the DNA damage marker γ-H2AX. As exhibited in Fig. 9a, HCECs exposed to 60 s of blue-violet light (405 nm, 25 mW/cm^2) used in this study showed the same minimal γ-H2AX expression as cells that were not exposed to the light. Afterward, cellular DNA damage gradually increased with a longer light duration. Therefore, a light curing time of 30 s was chosen for the following experiments.

Subsequently, co-staining with Calcein-AM and PI was used to further investigate the surface cytocompatibility of the FHATB hydrogel. In contrast to the culture plate, cell growth on the FHTAB hydrogel surface was sphere-shaped instead of spreading growth, which is because it had an elastic and hydrophilic surface (Fig. 9b). The surface of the FHTAB hydrogel significantly reduced the number of cells that remain on the surface, showing a certain anti-adhesive effect. Meanwhile, a few dead cells were observed in the FHTAB hydrogel group (containing Ag NPs), which may be caused by the localized high concentration formed on the contact surface of the cells with the hydrogel.

To examine whether the added components in the hydrogel affect the cell activity, several treatments were set up, which are hydrogel FH, hydrogel FHTA, and hydrogel FHTAB. Cell viability was assessed by co-culturing the cells with hydrogel extracts, and then by utilizing CCK-8. According to Fig. 9c, there was no significant difference in cell activity between groups when cells were cultured with hydrogel extracts of FH,

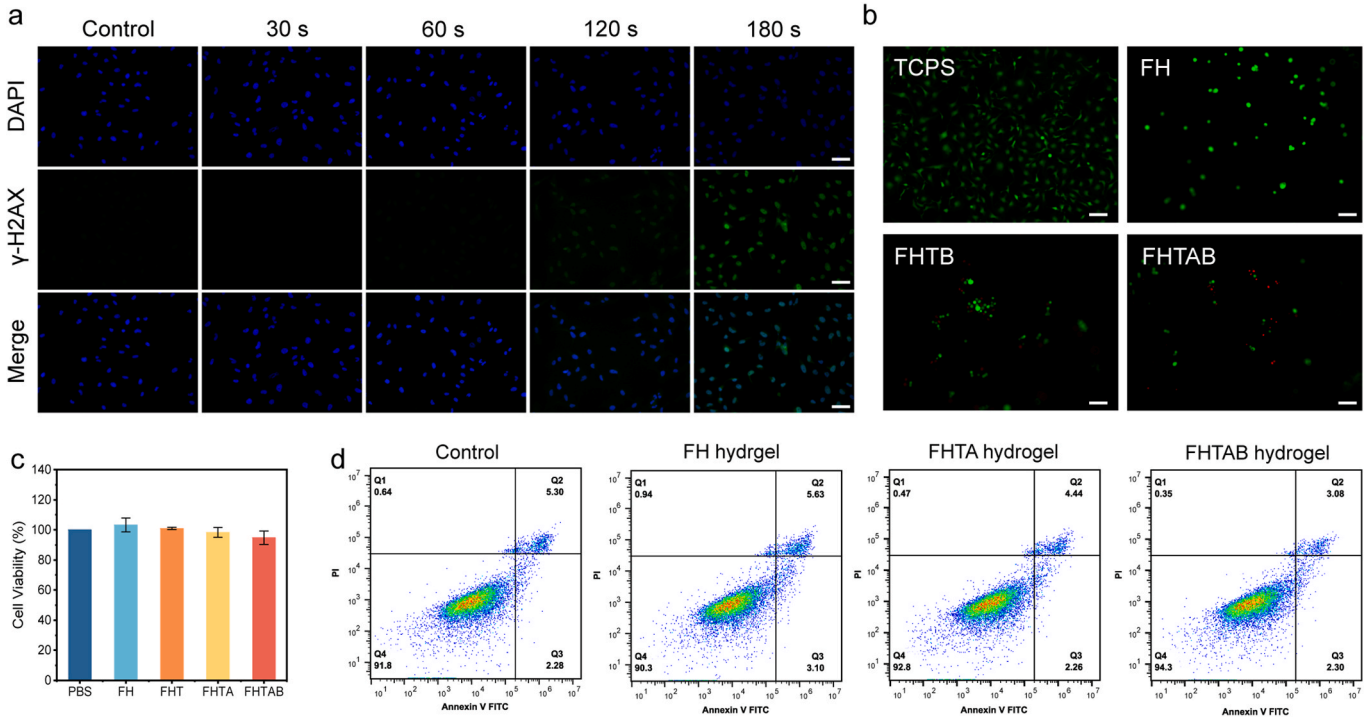

Fig. 9. Biocompatibility of FHTAB hydrogel. (a) Phototoxicity of 405 nm light with irradiation time (Scale bar = 100 μm). (b) Surface cytocompatibility of FHATB hydrogel (Scale bar = 100 μm). (c) Cytotoxicity of 7 d FHTAB hydrogel extracts. (d) Apoptosis induced by FHTAB hydrogel extracts.

FHTA and FHTAB. Apoptosis was also subsequently analyzed by flow cytometry. As shown in Fig. 9d, the added components in the hydrogel did not significantly induce early apoptosis.

3.12. FHTAB IOL implantation

According to the vitro physical properties performance and biocompatibility testing of FHTAB IOL, it was determined that the FTHAB IOL was operated as pre-heated (Fig. S2, Video 3). The rabbits were subjected to an ultrasound emulsification surgery first to obtain an empty capsular bag, which did not contain any lens tissue. The pre-heated FHTAB hydrogel precursor fluid completed the thermal gelation transition in a sterile syringe. Subsequently, it was carefully inserted into the empty lens capsule in the eye and immediately cured with 405 nm blue-violet light for 20 s (Video 4). As shown in Fig. 10a, the slit-lamp images reveal FHTAB IOL after photo-curing process. It showed considerable transparency and integrity in the fluid-rich intraocular environment. The FHTAB IOL was located in the capsular, not in the anterior chamber of the eye. Subsequently, the intraocular condition after FHTAB implantation was evaluated using anterior segment optical coherence tomography (AS-OCT) and all intraocular tissue structures are marked using different colors (Fig. S3). The eyes in non-operated group exhibited typical structures of the anterior segment with the cornea, the iris, lens capsule and natural lens clearly visible (Fig. S3a). Similarly, the intraocular structures described above were observed in the surgical group and the lens capsule was also shown as an upwardly

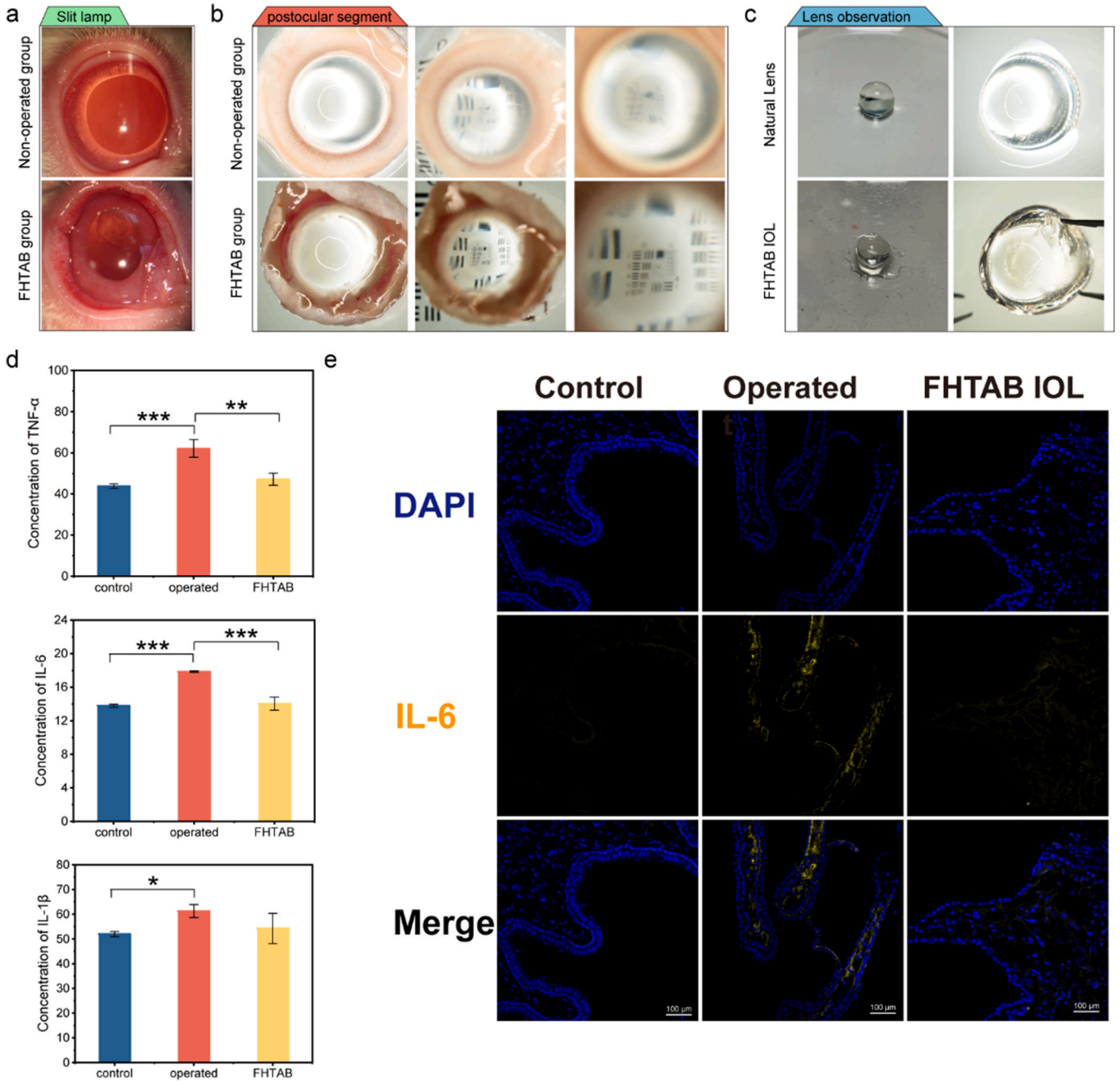

Fig. 10. Results of animal experiments on the implantation of FHTAB IOL in the eye of rabbits. (a) Slit lamp images of FHTAB IOL implantation eye and non-operated eye. (b) Evaluation of imaging and focusing performance of FHTAB IOL from the posterior segment of the eye. (c) General Observations on natural lens and FHTAB IOL removed from animal eyes. (d) Inflammatory factor levels in atrial fluid by ELISA. (e) IL-6 immunofluorescence tissue image of iris tissue.

convex arc, which means the FHTAB IOL was located inside the lens capsule (Fig. S3b). Moreover, the curve of the lens capsule membrane in OCT images was smooth, indicating that the process of in situ formation of FHTAB IOLs within the lens capsule could form the surface curvature of the natural lens. Also, the inflammatory response that occurred after surgery was also observed in the OCT images, which was marked with blue color. After the animal was euthanized, the eyeball was dissected into two parts based on the anterior and posterior segments of the eye. There was a view of the morphology of the FHTAB IOL in the posterior segment vision (Fig. 10b). Apposition between FHTAB IOL and posterior lens capsule membrane appeared tight, and there was no obvious breakage detected. Moreover, this IOL could be used to focus the image of a visual target in front of the eye. Finally, both natural lens and implanted FHTAB IOL were removed from the eyeballs. Compared with natural lens, FHTAB IOL was also a relatively regular ellipsoid, it had a smooth surface and was uniform throughout with no visible delamination (Fig. 10c). An undulating surface was found at the capsule crevasse, which was a limitation due to the syringe-pushing process. However, this problem can be solved by moving the capsule crevasse away from the refractive center or by developing a complementary injection device. Then the morphology of the FHTAB IOL was then filmed for analysis, by constantly zooming in on its surface. As shown in Fig. S4, FHTAB surfaces remained flat even at large magnifications.

Supplementary video related to this article can be found at https://doi.org/10.1016/j.bioactmat.2024.07.005

The postoperative inflammatory response is a prevalent issue in all intraocular surgeries, with a particularly high prevalence in cataract surgery. These inflammatory reactions are primarily caused by intraocular mechanical damage, chemical irritation, excess cortical residue and bacterial infection. In addition to stimulating the proliferation of

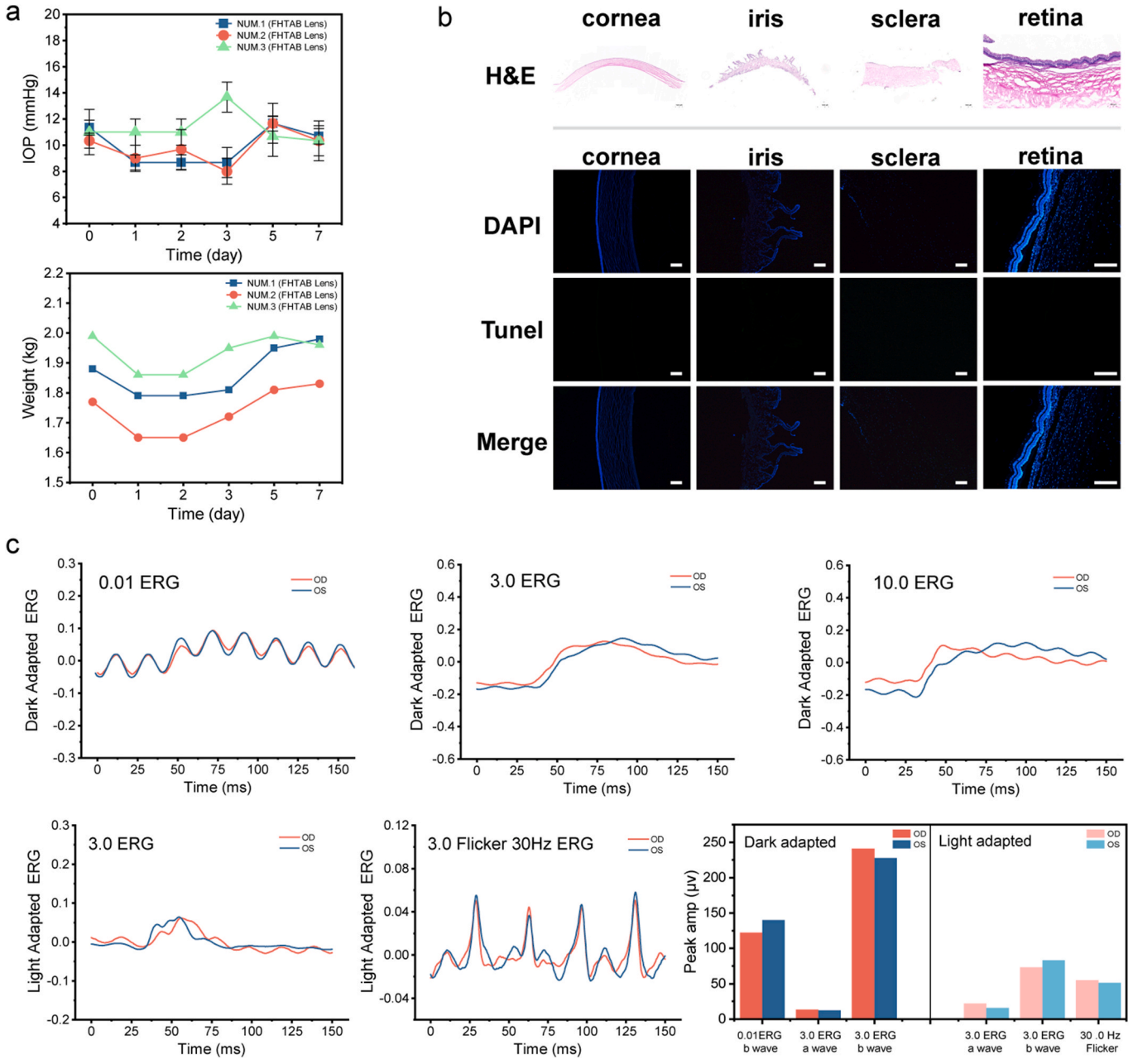

Fig. 11. In vivo biocompatibility of FHTAB IOL. (a) The 7 days IOP and weight changes of FHTAB IOL implantation eyes. (b) H&E-stained sections and Tunel-stained results of other tissues of the eye after FHTAB IOL implantation (c)The ERG data from FHTAB IOL implantation eye (OD) and non-surgical eye (OS) of the same rabbit.

HLECs remaining in the capsular, severe cases can lead to the formation of an inflammatory organized membrane. Therefore, postoperative anti-inflammatory and anti-bacterial therapy are necessary. The in vivo anti-inflammatory effect of FHTAB IOL was further evaluated by ELISA kit and immunofluorescence staining. The inflammatory factor levels were examined by extracting the atrial fluid of the experimental rabbits. As shown in Fig. 10d, the postoperative inflammatory factor level in the operated group was increased, whereas those in the FHTAB IOL implantation group decreased to some degrees. Then, the expression of IL-6 was examined by immunofluorescent staining of the iris. The results in Fig. 10e showed that the IL-6 expression level increased in the surgical group, whereas it was similar between the control group and FHTAB IOL group. These results suggested that FHTAB IOL also had anti-inflammatory effects in vivo.

Animals implanted with FHTAB IOL were also evaluated for IOP and body weight. According to Fig. 11a, in the group of animals with FHTAB IOL implantation, the IOP remained stable within a narrow range for seven consecutive days. This also suggested that a small amount of swelling of FHTAB IOL did not cause significant damage to IOP. In terms of weight, there was a slight decrease in weight during the first two days after the operation, followed by an increase. This could be the effect of the surgical act itself on the animal.

H&E staining and Tunel staining were also performed on other tissues in the eye after FHTAB lens implantation, including the cornea, iris, sclera, and retina. The results in Fig. 11b showed no obvious structural abnormalities in these tissues after FHTAB lens implantation. Additionally, the Tunel staining showed that FHTAB lens did not induce apoptosis in eye tissues.

The ERG was also operated to assess the overall retinal function following implantation of the FHTAB IOL. According to the ERG data from FHTAB IOL implantation eye (OD) and non-surgical eye (OS) of the same rabbit, there were no abnormal waveforms detected in the OD eye whether in light or dark adaptation (Fig. 11c). In light adapted ERG test, the amplitudes of the a-wave and b-wave in the right implanted eye were similar to those in the healthy contralateral eye. This indicated that the overall function of the retinal cone system is normal. On the other hand, the examination of the dark adapted ERG showed similar results, which reveal the fact that FHTAB IOL would not affect the overall function of the optic rod cells. Notably, the 10.0 ERG waveform is nearly identical to the 3.0 ERG, indicating that the refractive medium in the FHTAB IOL implanted eye was in a normal state. All the above results demonstrated that FHTAB IOL not only served as a refractive medium in the eye but also exhibited excellent intraocular biocompatibility.

4. Conclusion

This study successfully prepared a hydrogel-based FHTAB IOL as a natural lens substitute. FHTAB IOL were formed in capsule by a combination of thermos-gelation and photo-curing strategies. It had high transparency, optical transmittance, similar refractive index of natural lens and a certain degree of adjustability. The animal experiments also confirmed that it could stabilize as a refractive medium in the eyes after surgery and had good biocompatibility. By loaded with Ag NPs and TA, FHTAB IOL showed significant vivo and in vivo antibacterial and anti-inflammatory effects, which could effectively reduce the risk of post-operative intraocular infection and inflammation. This study also offered new insights into the advancement of adjustable IOLs and natural lens substitutes.

5. Ethics approval and consent to participate

The animal experiments were approved by the Committee and Laboratory Animal Center of Eye Hospital, Wenzhou Medical University. The ethical approval Number was YSG23102613.

CRediT authorship contribution statement

Chen Qin: Writing – original draft, Validation, Software, Methodology, Investigation, Formal analysis. **Fan Fei:** Methodology, Investigation, Formal analysis. **Youfei Wei:** Methodology, Investigation, Data curation. **Yuemei Han:** Validation, Supervision, Methodology. **Di Hu:** Validation, Software. **Quankui Lin:** Writing – review & editing, Supervision, Project administration, Funding acquisition, Formal analysis, Conceptualization.

Declaration of competing interest

The authors have declared that no competing interest exists.

Acknowledgments

This work was financially supported by the Zhejiang Provincial Natural Science Foundation [LR23H180001] and the Key Scientific and Technological Innovation Projects in Wenzhou [ZY2021002].

Appendix A. Supplementary data

Supplementary data to this article can be found online at https://doi.org/10.1016/j.bioactmat.2024.07.005.

References

[1] L.Z. Ma, Y.R. Zhang, Y.Z. Li, et al., Cataract, cataract surgery, and risk of incident dementia: a prospective cohort study of 300,823 participants, Biol. Psychiatr. 93 (9) (2023) 810–819.
[2] R. Narang, A. Agarwal, Refractive cataract surgery, Curr. Opin. Ophthalmol. 35 (1) (2024) 23–27.
[3] M.V. Cicinelli, J.C. Buchan, M. Nicholson, et al., Cataracts, Lancet 401 (10374) (2023) 377–389.
[4] T. Lapp, K. Wacker, C. Heinz, et al., Cataract surgery-indications, techniques, and intraocular lens selection, Dtsch. Arztebl. Int. 120 (21) (2023) 377–386.
[5] H. Bhattacharjee, S. Mishra, M. Garg, Pseudoexfoliative deposits on an intraocular lens, JAMA Ophthalmol. 141 (6) (2023) 230407.
[6] C. Qin, S. Wen, F. Fei, et al., NIR-triggered thermosensitive polymer brush coating modified intraocular lens for smart prevention of posterior capsular opacification, J. Nanobiotechnol. 21 (2023) 323.
[7] X. Zhang, J. Wang, J. Xu, et al., Prophylaxis of posterior capsule opacification through autophagy activation with indomethacin-eluting intraocular lens, Bioact. Mater. 23 (2023) 539–550.
[8] Y. Hu, J. Wang, Y. Hong, et al., Photo-controllable drug releasing bulk polyacrylic intraocular lens material for safer posterior capsular opaciffcation prevention, J. Contr. Release 366 (2024) 494–504.
[9] J. Wang, Y. Hu, Y. Han, et al., Non-viral gene coating modified IOL delivering PDGFR-α shRNA interferes with the fibrogenic process to prevent posterior capsular opacification, Regen.Biomater. 10 (2023) rbad020.
[10] S. Zhu, H. Huang, D. Liu, et al., Augmented cellular uptake and homologous targeting of exosome-based drug loaded IOL for posterior capsular opacification prevention and biosafety improvement, Bioact. Mater. 15 (2022) 469–481.
[11] D. Lu, Y. Han, D. Liu, et al., Centrifugally concentric ring-patterned drug-loaded polymeric coating as an intraocular lens surface modification for efficient prevention of posterior capsular opacification, Acta Biomater. 138 (15) (2022) 327–341.
[12] D. Lu, H. Wang, C. Feng, et al., Spin coating based facile annular photodynamic intraocular lens fabrication for efficient and safer posterior capsular opacification prevention, ACS Appl. Mater. Interfaces 14 (43) (2022) 48341–48355.
[13] Y. Hong, D. Liu, H. Zou, et al., Refractive index adjustable intraocular lens design to achieve diopter control for improving the treatment of ametropia after cataract surgery, Acta Biomater. 178 (2024) 124–136.
[14] J.L. Alio, F. D'Oria, F. Toto, et al., Retinal image quality with multifocal, EDOF, and accommodative intraocular lenses as studied by pyramidal aberrometry, Eye Vis.(Lond). 8 (1) (2021) 37.
[15] J. Ford, L. Werner, N. Mamalis, Adjustable intraocular lens power technology, J. Cataract Refract. Surg. 40 (7) (2014) 1205–1223.
[16] H.B. Dick, R.D. Gerste, Future intraocular lens technologies, Ophthalmology 128 (11) (2021) 206–213.
[17] X. Hao, J.L. Jeffery, T.P. Le, et al., High refractive index polysiloxane as injectable, in situ curable accommodating intraocular lens, Biomaterials 33 (23) (2012) 5659–5671.
[18] D.J. Apple, J. Sims, Harold Ridley and the invention of the intraocular lens, Surv. Ophthalmol. 40 (4) (1996) 279–292.
[19] Y. Hong, Q. Fang, T. Bai, et al., Cascade reaction triggering and photothermal AuNPs@MIL MOFs doped intraocular lens for enhanced posterior capsular opacification prevention, J. Nanobiotechnol. 21 (2023) 134.

[20] D. Liu, J. Tang, L. Shen, et al., Foldable bulk anti-adhesive polyacrylic intraocular lens materials design and fabrication for posterior capsule opacification prevention, Biomacromolecules 23 (4) (2022) 1581–1591.
[21] Y. Hong, H. Zou, Y. Hu, et al., Foldable, responsively drug eluting polyacrylic intraocular lens bulk materials design for postoperative complications prevention, J. Mater. Chem. B 10 (2022) 8398–8406.
[22] P.J. May, P.D. Gamlin, Is primate lens accommodation unilaterally or bilaterally controlled? Invest. Ophthalmol. Vis. Sci. 61 (8) (2020) 5.
[23] W. Zhang, T. Peng, X. Cheng, et al., Comparison of postoperative visual performance between trifocal intraocular lens and monofocal intraocular lens, Saudi Med. J. 44 (5) (2023) 456–462.
[24] A. Sauer, T. Bourcier, D. Gaucher, et al., Intraocular cytokines imbalance in congenital cataract and its impact on posterior capsule opacification, Clin. Exp. Ophthalmol. 254 (5) (2016) 1013–1018.
[25] J. Gao, M. Li, J. Cheng, et al., 3D-Printed GelMA/PEGDA/F127DA scaffolds for bone regeneration, J. Funct. Biomater. 14 (2) (2023).
[26] H. Jafari, P. Ghaffari-Bohlouli, S.V. Niknezhad, et al., Tannic acid: a versatile polyphenol for design of biomedical hydrogels, J. Mater. Chem. B 10 (31) (2022) 5873–5912.
[27] K. Wu, M. Fu, Y. Zhao, et al., Anti-oxidant anti-inflammatory and antibacterial tannin-crosslinked citrate-based mussel-inspired bioadhesives facilitate scarless wound healing, Bioact. Mater. 20 (2023) 93–110.
[28] Y. Xu, S. Chen, Y. Zhang, et al., Antibacterial black phosphorus nanosheets for biomedical applications, J. Mater. Chem. B 11 (30) (2023) 7069–7093.
[29] Y. Zhang, J. Kang, X. Chen, et al., Ag nanocomposite hydrogels with immune and regenerative microenvironment regulation promote scarless healing of infected wounds, J. Nanobiotechnol. 21 (1) (2023) 435.
[30] M. Rong, J. Liu, Z. Sun, et al., Rational utilization of black phosphorus nanosheets to enhance palladium-mediated bioorthogonal catalytic activity for activation of therapeutics, Angew. Chem. Int. Ed. 62 (19) (2023) 202216822.
[31] L. Pan, X.-D. Zhu, K.-N. Sun, et al., Molecular level distribution of black phosphorus quantum dots on nitrogen-doped graphene nanosheets for superior lithium storage, Nano Energy 30 (2016) 347–354.
[32] R. Wang, X. Jin, Q. Wang, et al., A transparent, flexible triboelectric nanogenerator for anti-counterfeiting based on photothermal effect, Matter 6 (5) (2023) 1514–1529.
[33] H. Tanabe, T. Shojo, K. Takase, et al., Comparison of visual performance between non-tinted and yellow-tinted monofocal intraocular lenses of the same material and basic design, Invest. Ophthalmol. Vis. Sci. 63 (7) (2022) 2879.
[34] J. Maule, A.E. Skelton, A. Franklin, The development of color perception and cognition, Annu. Rev. Psychol. 74 (2023) 87–111.
[35] B.A. Altmann, J. Gertheiss, I. Tomasevic, et al., Human perception of color differences using computer vision system measurements of raw pork loin, Meat Sci. 188 (2022) 108766.
[36] M. Zhang, Y. Zhang, Z. Jiang, et al., Low-illumination image enhancement in the space environment based on the DC-WGAN algorithm, Sensors 21 (1) (2021).
[37] H. Fukuoka, H.E. Gali, J.J. Bu, et al., Ultraviolet light exposure and its penetrance through the eye in a porcine model, Int. J. Ophthalmol. 16 (2) (2023) 172–177.